Tellus SERIES A DYNAMIC METEOROLOGY AND OCEANOGRAPHY
PUBLISHED BY THE INTERNATIONAL METEOROLOGICAL INSTITUTE IN STOCKHOLM

Tellus (2008), 60A, 1079–1088
Printed in Singapore. All rights reserved

TELLUS

Linear amplification of marginally neutral baroclinic waves

By HYLKE DE VRIES* and MARTIN EHRENDORFER, *University of Reading, Department of Meteorology, PO BOX 243, Earley Gate, Reading. RG6 6BB, United Kingdom*

(Manuscript received 31 January 2008; in final form 27 June 2008)

ABSTRACT

Baroclinic wave development is investigated for unstable parallel shear flows in the limit of vanishing normal-mode growth rate. This development is described in terms of the propagation and interaction mechanisms of two coherent structures, called counter-propagating Rossby waves (CRWs). It is shown that, in this limit of vanishing normal-mode growth rate, arbitrary initial conditions produce sustained linear amplification of the marginally neutral normal mode (mNM). This linear excitation of the mNM is subsequently interpreted in terms of a resonance phenomenon. Moreover, while the mathematical character of the normal-mode problem changes abruptly as the bifurcation point in the dispersion diagram is encountered and crossed, it is shown that from an initial-value (CRW) viewpoint, this transition is smooth. Consequently, the resonance interpretation remains relevant (albeit for a finite time) for wavenumbers slightly different from the ones defining cut-off points. The results are further applied to a two-layer version of the classic Eady model in which the upper rigid lid has been replaced by a simple stratosphere.

1. Introduction

Many baroclinic and barotropic shear flows support a discrete spectrum of neutral and exponentially amplifying wave-like disturbances, called normal modes (NMs). NMs are solutions of the linearized dynamic equations, with time-independent structure. It has long been recognized, for instance, through the work of Eady (1949) and Charney (1947), that growing NMs—in particular the most rapidly growing NM—play an important role in the problem of extratropical cyclogenesis. Necessary conditions for the existence of a growing and decaying NM (gNM and dNM, respectively) are a sign-change in the basic-state potential vorticity gradient $\bar{q}_y$ (the Charney–Stern condition; Charney and Stern, 1962) and a positive correlation between the zonal wind $\bar{u}$ and $\bar{q}_y$ (Fjørtoft, 1951).

However, even if both necessary conditions for instability are satisfied, existence of a gNM for all zonal wavenumbers is not guaranteed. The Eady (1949) model is a classic example. In Eady-like geometries (*f*-plane, piecewise constant shear and buoyancy frequency), the dynamics is determined solely from meridional displacements at boundaries and interfaces. A short-wave cut-off appears because the Rossby height decreases with increasing wavenumber. A long-wave cut-off may also exist. This happens, for instance, if one replaces the upper rigid lid of the classic Eady model by a simple stratosphere (Müller, 1991). The dispersion curves of the Charney (1947) and Green (1960) models also show cut-off wavenumbers and/or neutral points.

The present paper has its focus on those regions of the dispersion diagram (of which an example is shown in Fig. 1) where the NM growth rate tends to zero. Why would those regions be interesting and important to consider? Two main reasons are stated below.

First, time-invariance of the inviscid dynamic equations implies that the gNM and dNM have identical phase speeds but complex conjugate vertical structures and growth rates. Consequently, the gNM and dNM become identical at an instability cut-off point; they 'merge' into a single marginally neutral NM (mNM). It follows that the two-dimensional system is underdetermined in the sense that inclusion of a so-called secular term is required under these circumstances (Boyce and DiPrima, 2003). This secular term produces linear or, more generally, algebraic growth, which can be interpreted as a resonance. Since algebraic (linear) growth can be faster than exponential growth on relatively short time intervals, enhanced insight into the mNM may be relevant for short-term baroclinic development, as well as for systems that are weakly unstable. The principal aim of this paper is to investigate this resonance phenomenon.

There is, however, a second reason why we think it is important to have a good physical understanding of the mNM and its excitability. This reason is that the mNM connects two parts of the dispersion curve (i.e. regions of phase-space) that have qualitatively very different NM dynamics (exponentially

*Corresponding author.
e-mail: h.devries@reading.ac.uk
DOI: 10.1111/j.1600-0870.2008.00355.x

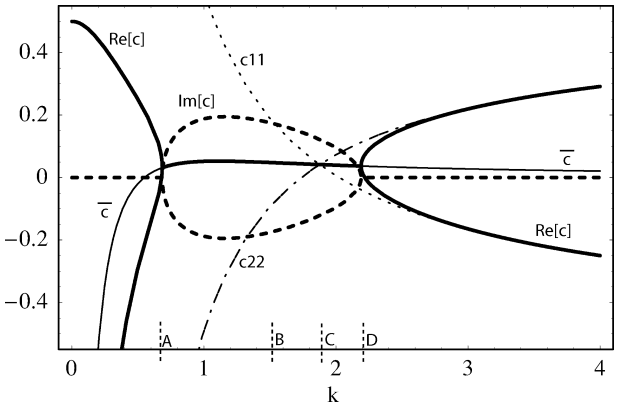

Fig. 1. Dispersion diagram for the two-layer Eady model. Specific wavenumbers discussed in the text: (A) long-wave cut-off ($k = 0.68$); (B) most-unstable wave ($k = 1.55$); (C) 'resonantly' unstable wave ($k = 1.88$)and (D) Short-wave cut-off ($k = 2.19$).

amplifying/decaying waves versus neutral oscillations). The fact that it is the (linearly amplifying) mNM that forms this connection, could perhaps be anticipated from NM analysis (one might argue for instance that $\exp(\hat{\sigma}t) \sim 1 + \hat{\sigma}t$ for small growth rate $\hat{\sigma}$) but is still not trivial since the growth rate $\hat{\sigma}$ vanishes exactly in the marginal limit. The second aim of the paper is to show that this connection can, however, readily be demonstrated and made understandable by adopting an initial-value viewpoint. More specifically, although the normal-mode problem changes abruptly when a bifurcation point is crossed in the dispersion diagram, it will be shown that from an initial-value perspective, this transition is completely smooth. Mathematical details and examples are provided to underpin this statement further.

We consider the above mathematical questions about the dispersion diagram in the context of a physical model of the atmosphere (such as the Eady model). By this, the relevance of the results discussed here for real atmospheric situations is emphasized.

We will now briefly outline what methods will be used. The NMs provide a precise mathematical way to describe baroclinic development. However, it is more difficult to use them to reveal the physical mechanisms underlying the development from more general initial conditions. The qualitatively powerful potential vorticity (PV) perspective (Hoskins et al., 1985), for instance, is not used in a modal description, and this makes the interpretation and robust qualitative prediction from general initial conditions often difficult.

An alternative description of the dynamics is in terms of so-called counter-propagating Rossby waves (CRWs; Heifetz et al., 2004a; Methven et al., 2005). The CRW perspective constitutes a concise theory for interpreting both modal and non-modal baroclinic development in terms of the propagation and interaction of just two coherent structures—the two CRWs. Evolution from initial conditions consisting of arbitrary linear combinations of gNM and dNM then can be interpreted in exactly the same way as baroclinic development in the classic Eady (1949) problem is usually understood, namely in terms of two interacting edge waves (Davies and Bishop, 1994). In contrast to a description in NMs, the CRW description takes full advantage of the PV perspective. In the case of the Eady (1949) model, the CRWs take the simple form of pure surface and tropopause potential temperature anomalies (boundary edge waves). In more complex geometries where the interior mean PV gradient is non-zero, the CRWs have a more complex structure (Heifetz et al., 2004b). CRW-theory is general in so far as that it is applicable to any (inviscid) baroclinic/barotropic model that supports a gNM–dNM pair. For a more complete introduction to CRW-theory, we refer to Heifetz et al. (2004a).

The CRW framework is briefly discussed in Section 2. Section 3 describes the resonance. The theory is applied to a two-layer version of the Eady (1949) model in Section 4. Concluding remarks follow in Section 5.

2. CRW equations

The quasi-geostrophic (QG) system is now used to explain how CRWs can be constructed. In QG theory the evolution of small perturbations is described by the linearized QG, PV equation

$$q_t + \bar{u}q_x + v\bar{q}_y = 0, \tag{1}$$

where q denotes the perturbation PV and (u, v) denote the horizontal wind in the zonal (x) and meridional (y) directions, respectively. Mean-state variables carry a bar. The potential temperature boundary conditions have been included as PV delta functions as in Bretherton (1966).

In the following, it is assumed that a gNM can be obtained (even if the growth rates are small) by solving (1) for a sufficiently long time.

2.1. CRWs

CRWs are special linear combinations of the gNM and its complex conjugate, the dNM. Heifetz et al. (2004a) describe two methods how they can be obtained: the 'home-base' method and the 'orthogonality' method. In this paper, we adopt the home-base method. This choice is convenient if the mean PV gradient has a simple structure.

The CRWs are constructed in the following way. Let the PV structure of the gNM be denoted by q_g. Because the gNM and dNM (with PV structure $q_d \equiv q_g^*$) tilt in opposite directions, the combination $bq_g + b^*q_d$ will be vertically un-tilted (b can be any complex constant). Using the invertibility principle, the meridional wind field will also be un-tilted and in quadrature with the PV (Hoskins et al., 1985). It follows that this PV structure is neutral and self-propagating. The upper CRW (CRW-2) is defined by choosing the complex constant b such that the resulting structure has zero PV signature at the surface. The lower CRW (CRW-1) is defined to have zero PV signature at the level

at which CRW-2 attains its PV maximum. This level is called the home base of CRW-2, and for obvious reasons, the surface is called the home base of CRW-1.

The lower and upper CRW are labelled by subscripts 1 and 2, respectively: $q_{1,2}(z)$ denote the PV structures and $v_{1,2}(z)$ the meridional winds. We limit ourselves to initial conditions formed by CRWs only (or, equivalently, to gNM–dNM superpositions only). Any perturbation PV state at time t can then be written as $q(z, t) = \alpha_1(t)q_1(z) + \alpha_2(t)q_2(z)$. The complex factor α_i is further expressible in a real amplitude $a_i(t)$ and phase $\epsilon_i(t)$ of the CRW

$$\alpha_{1,2}(t) \equiv a_{1,2}(t)\mathrm{e}^{\mathrm{i}\epsilon_{1,2}(t)}. \tag{2}$$

The linear evolution of this two-wave system is described by:

$$\begin{pmatrix}\dot{\alpha}_1\\ \dot{\alpha}_2\end{pmatrix} = -\mathrm{i}k\mathbf{A}\underbrace{\begin{pmatrix}\alpha_1\\ \alpha_2\end{pmatrix}}_{\equiv\boldsymbol{\alpha}}, \quad \mathbf{A} = \begin{pmatrix}c_{11} & c_{12}\\ c_{21} & c_{22}\end{pmatrix}. \tag{3}$$

The coefficients c_{ij} depend on the model geometry and on the properties of the perturbation, such as the zonal wavenumber k. The diagonal elements c_{11} and c_{22} of $\mathbf{A}$ determine the phase speeds of the lower and upper CRW in absence of interaction, respectively, and the off-diagonal elements describe their interaction (Heifetz et al., 2004a). If the home-base method is used for constructing the CRWs, the c_{ij} are given by

$$c_{ij} = \bar{u}_i\delta_{ij} - \frac{\gamma_{ij}}{k}, \qquad \gamma_{ij} = \left(\frac{v_j}{q_i}\frac{\partial\bar{q}}{\partial y}\right)\bigg|_{z_i}, \tag{4}$$

where $z_{1,2}$ mark the home bases of the two CRWs. The final step is to re-normalise the structure of the CRWs such that the interaction coefficients become equal and opposite:

$$c_{12} = -c_{21} \equiv \frac{\sigma}{k} > 0. \tag{5}$$

Note that the coefficients c_{ij} and their parameter dependence change if the orthogonality method were used instead of the home-base method, or if linearized primitive-equation dynamics were used. However, the structure of the two-wave equations, as written in (3) does not change. Therefore, the results obtained in the remainder of this section, as well as in Section 3 are valid in general.

2.2. Normal modes and exponential growth

Following Heifetz and Methven (2005) the matrix $\mathbf{A}$ is rewritten as

$$\mathbf{A} = \begin{pmatrix}\bar{c} + \frac{\mu}{2k} & \frac{\sigma}{k}\\ -\frac{\sigma}{k} & \bar{c} - \frac{\mu}{2k}\end{pmatrix}, \tag{6}$$

where $\bar{c} \equiv \frac{1}{2}(c_{11} + c_{22})$ is the mean of the self-propagation speeds of the two CRWs and $\mu \equiv -k(c_{22} - c_{11})$ is proportional to their difference. The NMs are obtained as the eigenvectors of $\mathbf{A}$. The eigenvalues are

$$c_\pm = \bar{c} \pm \frac{\sigma}{k}\sqrt{\Gamma}, \qquad \Gamma \equiv \rho^2 - 1, \tag{7}$$

where $\rho \equiv \mu/(2\sigma)$. Unstable waves ($\Gamma < 0$) propagate zonally with speed $\bar{c}$, have CRW amplitude ratio $\chi \equiv a_2/a_1 = 1$. The CRW phase-difference $\epsilon \equiv \epsilon_2 - \epsilon_1 = \epsilon_+$ in the gNM is given by $\cos(\epsilon_+) = -\rho$ ($0 \le \epsilon_+ \le \pi$) and the gNM growth rate is $k\mathrm{Im}(c) = \hat{\sigma} \equiv \sigma\sin(\epsilon_+)$.

3. Marginally neutral waves

3.1. The cut-off condition

If an instability cut-off wavenumber k_c is found in the dispersion diagram, it satisfies $\Gamma = 0$ following (7), further implying that $\rho = \rho_c$ where

$$\rho_c \equiv \frac{\mu_c}{2\sigma_c} = \pm 1, \tag{8}$$

where $\mu_c \equiv \mu|_{k=k_c}$ and $\sigma_c \equiv \sigma|_{k=k_c}$. The factor ρ_c is introduced to simplify notation and arises because μ can be either positive or negative at an instability cut-off. The physical interpretation here is that, at the cut-off wavenumber, either the upper ($-$) or the lower ($+$) CRW propagates fastest in the zonal (eastward) direction. In the Eady problem, for instance, the short-wave cut-off is obtained when $\rho_c = -1$ (i.e. $\mu < 0$ and $c_{22} > c_{11}$).

From (7), it also follows that if $\Gamma = 0$, there is only one eigenvalue $c = \bar{c}$ with multiplicity 2. There is also only one eigenvector, which has the form $(\alpha_1, \alpha_2) = (-\rho_c, 1)$. This eigenvector is the mNM, in which the CRWs phase-lock either with zero phase-difference (if $\rho_c = -1$) or with a phase-difference equal to π (if $\rho_c = 1$).

Clearly, the gNM and dNM have become identical. Therefore, at this wavenumber, the NMs—or, more precisely, the single NM—cannot describe correctly the evolution from initial conditions with arbitrary upper and lower CRW.[1] What then happens with such initial conditions in this limit?

As already announced in Section 1, it turns out that such initial conditions trigger a resonance-like phenomenon as a result of which the amplitude of the mNM increases linearly with time. Mathematically, the behaviour of the system under these circumstances is well understood (Boyce and DiPrima, 2003): the inclusion of a secular term proportional to t is needed if the eigenvalue has multiplicity 2, and there is only one associated eigenvector. The physics of the resonance can be understood as follows. The mNM itself is a neutral solution of the equations. Any initial condition differing from this mNM can use part of its wind field to excite the mNM. Since there is no feedback from the mNM to the initial condition, the growth is linear and, in principle, unbounded (as long as friction is ignored). The above

[1] Since the CRWs require the existence of the gNM, their construction can be difficult in the limit of vanishing growth rate.

reasoning is illustrated by showing the underlying mathematical structure of the solutions.

3.2. Conditions for linear growth

It is instructive to verify that the conditions leading to linear growth are indeed the marginal neutrality conditions. To this aim, we first reduce (3) to a single second-order equation

$$\ddot{\alpha} - p\dot{\alpha} + q\alpha = 0, \tag{9}$$

where $\alpha = \alpha_{1,2}$, $p = \mathrm{tr}(-\mathrm{i}k\mathbf{A})$ and $q = \det(-\mathrm{i}k\mathbf{A})$. Substituting a trial solution $\alpha(t) = f(t)\exp(\omega t)$ ($\omega \equiv -\mathrm{i}kc_{nm}$ relates to the yet unknown propagation speed c_{nm} of the mode) gives

$$\ddot{f} + \underbrace{(2\omega - p)}_{r_1}\dot{f} + \underbrace{(\omega^2 - p\omega + q)}_{r_0} f = 0. \tag{10}$$

Linear growth occurs if both r_1 and r_0 are zero. Setting $r_1 = 0$ implies that $c_{nm} = \bar{c}$, the propagation speed of all unstable normal modes. Using this relation and setting $r_0 = 0$ gives $p^2 = 4q$, which indeed is satisfied if the condition for marginal neutrality ($\Gamma = 0$) holds.

3.3. Analytic solution in Jordan space

As long as $\Gamma \neq 0$, system (3) can always be transformed into diagonal form, implying that the solution can be written as a linear superposition of two independent eigenvectors (normal modes). On the other hand, if $\Gamma = 0$ we have seen that there is just one eigenvector (the mNM). In that case, system (3) can no longer be written in completely diagonal form, and off-diagonal terms appear. These off-diagonal terms give rise to algebraic growth. To see this more explicitly, it may be verified that one can rewrite (3) for $\Gamma = 0$ as

$$\dot{\boldsymbol{\beta}} = (-\mathrm{i}k)\mathrm{J}\boldsymbol{\beta} \quad \mathbf{J} = \begin{pmatrix} \bar{c} & 1 \\ 0 & \bar{c} \end{pmatrix}, \tag{11}$$

where $\boldsymbol{\beta} \equiv \mathbf{T}^{-1}\,\boldsymbol{\alpha}$ (see Appendix A for the definition of the transformation matrix $\mathbf{T}$) and $\mathbf{J}$ is the so-called *Jordan* matrix (Boyce and DiPrima, 2003). We refer to (11) as the 'neutral CRW equations in Jordan space'. Their solution is given by

$$\boldsymbol{\beta}(t) = \mathrm{e}^{-\mathrm{i}k\bar{c}t}\begin{pmatrix} 1 & -\mathrm{i}kt \\ 0 & 1 \end{pmatrix}\boldsymbol{\beta}(0), \tag{12}$$

giving explicitly the form of $\exp(-\mathrm{i}k\mathbf{J}t)$. Considering the solution in Jordan space clearly shows that the linearly growing part vanishes only in the trivial situation (for the initial condition identical zero) or when $\beta_2(0)$ vanishes. By the definition of $\boldsymbol{\beta}$ and referring to the structure of $\mathbf{T}$ (see eq. A1), vanishing $\beta_2(0)$ implies that the initial PV structure is precisely equal to the mNM, which simply propagates with $\bar{c}$, and is thus unable to excite a resonance.

Conversely, whenever $\beta_2(0) \neq 0$, implying that the initial condition is different from the mNM, it is seen from (12) that this initial condition 'excites' a linearly growing contribution to β_1 (which represents the mNM in the solution). Thus, as discussed further below, at long times, the solution is in this resonating situation dominated by the linearly growing structure of the mNM.

3.4. Analytic solution in CRW space

We now return to the solution in CRW space. Given (12), the solution of the original system (3) becomes[2]

$$\alpha_1(t) = [B_0 - \mathrm{i}\sigma t(T_0 + \rho_c B_0)]\mathrm{e}^{-\mathrm{i}k\bar{c}t}, \tag{13}$$

$$\alpha_2(t) = [T_0 + \mathrm{i}\sigma t(B_0 + \rho_c T_0)]\mathrm{e}^{-\mathrm{i}k\bar{c}t}, \tag{14}$$

where we have identified the initial conditions as $\alpha_1(0) \equiv B_0$ and $\alpha_2(0) \equiv T_0$. Note that, here and in Section 3.3, all parameters such as σ and μ are to be evaluated at the cut-off wavenumber k_c. As already seen from the solution in Jordan space, it is evident here again that the resonant part of the solution vanishes only in the trivial situation or when the initial condition is precisely equal to the mNM, that is, $T_0/B_0 = -\rho_c$. Similar to resonating continuum modes, the linearly amplifying parts are always $\pi/2$ out of phase with the initial anomalies (Davies and Bishop, 1994; De Vries and Opsteegh, 2005; Jenkner and Ehrendorfer, 2006) and the time-asymptotic structure of any initial condition is given by the mNM. Furthermore, the instantaneous CRW propagation speeds are not equal to $\bar{c}$, except in the time-asymptotic limit. Intriguing from a CRW-perspective is that the initial anomalies are not decaying in time whereas the mNM is amplifying.

Finally, it is perhaps worth mentioning that the above resonant solutions relate to the classical concept of forced harmonic oscillators. Hereto, note that (13) and (14) satisfy the following differential equations:

$$\ddot{\alpha}_1 + w_0^2\alpha_1 = -2\sigma(T_0 + \rho_c B_0)w_0\mathrm{e}^{-\mathrm{i}w_0 t}, \tag{15}$$

$$\ddot{\alpha}_2 + w_0^2\alpha_2 = \ 2\sigma(B_0 + \rho_c T_0)w_0\mathrm{e}^{-\mathrm{i}w_0 t}, \tag{16}$$

where $w_0^2 = (k\bar{c})^2$ is the natural frequency of the oscillators. Any initial perturbation (B_0, T_0) (at this particular cut-off wavenumber) produces resonant forcing to both oscillators (as long as $B_0 + \rho_c T_0 \neq 0$).

4. Example: Two-layer Eady model

This section applies the results of the previous sections to the two-layer Eady (1949) model discussed by Müller (1991). The basic state is formed by a zonal wind profile $\bar{u}(z)$, which has

[2] Another, more direct way to obtain (13) and (14), is to solve (3) for general initial conditions and parameters and subsequently take the limit $\Gamma \to 0$. For reference, the general solution is stated in (C12), in Appendix C.

constant but different shears $\Lambda_{s,t}$ in the stratosphere (subscript s) and troposphere (subscript t), and a buoyancy frequency profile $N^2(z)$, which discontinuously jumps from N_t^2 in the troposphere to N_s^2 in the stratosphere. The governing equation for the dynamics is the QG PV eq. (1). Since the *f*-plane approximation is made, the mean PV gradient $\bar{q}_y$ vanishes in the interior. At the lower boundary and the tropopause, however, the mean PV gradient is generally non-zero and can be written as

$$\bar{q}_y(z) = -\tilde{\Lambda}_t \delta(z - z_1) + (\tilde{\Lambda}_t - \tilde{\Lambda}_s)\delta(z - z_2), \tag{17}$$

where $\tilde{\Lambda}_{t,s} = \Lambda_{t,s} N_{t,s}^{-2}$. The surface and tropopause therefore mark the home bases of the two CRWs. CRW-1 assumes the form of a surface PV anomaly $q_1 \sim \delta(z - z_1)$ and CRW-2, that of a tropopause PV anomaly $q_2 \sim \delta(z - z_2)$. Wind fields associated with the CRWs are computed using Green's functions as in De Vries and Opsteegh (2007). Thereby, the interaction coefficients γ_{ij} (and μ and σ) are determined.

We use non-dimensional notation based on the scalings $U = 30$ m s^{-1}, $H = 10$ km (height of the tropopause above the ground), $L = 1000$ km and $N_0/f_0 = 100$ with $f_0 = 10^{-4}$ s^{-1} the Coriolis parameter (Pedlosky, 1987). The timescale is $T = L/U \sim 9.26$ h, such that five non-dimensional time units are approximately 48 h. In this paper, we take $\Lambda_{t,s} = \pm 1$ (in units U/H) and $N_s/N_t = 2$. These choices result in a tropopause mean PV gradient, which is positive and larger in amplitude than the (negative) surface mean-PV gradient (The classic Eady, 1949, problem with upper rigid lid, which results in the limit $N_s^2 \to \infty$, has equal and opposite PV gradients).

The NMs of the two-layer Eady model have first been discussed by Müller (1991) and more recently by De Vries and Opsteegh (2007). Some properties of the NMs are briefly discussed here by analysing the dispersion diagram (Fig. 1). The ground (home base of CRW-1) and tropopause (home base of CRW-2) are located at $z_1 = -\frac{1}{2}$ and $z_2 = +\frac{1}{2}$, respectively. This choice of frame of reference is convenient because it produces stationary non-dispersive gNMs in the classic Eady model with upper rigid lid. In the two-layer Eady model, however, the gNMs are no longer stationary (Fig. 1) but are seen to propagate slowly eastwards for the present choice of basic-state parameters.

The flow is unstable for a range of wavenumbers (dashed lines in Fig. 1). Within this range, there is one particular wavenumber for which the lower and upper CRW in isolation have identical phase-speeds, $c_{11} = c_{22}$ (denoted by point C in Fig. 1). Since no phase-speed adjustment is required to form a mode, as expected, the CRWs phase lock in the gNM with a $\epsilon = \pi/2$ phase difference. For this reason, one could call this the 'resonantly' unstable wave (De Vries and Opsteegh, 2007). The growth rate of this particular gNM is equal to the interaction coefficient itself, $\hat{\sigma} = \sigma$, because $\rho = 0$ in (7). Although it is the most natural wavenumber for the flow to become unstable (i.e. if $\sigma \sim 0$ in 7, only $\mu \sim 0$ can produce a gNM), the growth rate of the resonantly unstable wave is usually not the largest; in the present case (as well as in the classic Eady model and Charney model), the most unstable wave (point B in Fig. 1) is found at a smaller wavenumber.

Because the self-counter-propagation rates γ_{ii}/k decrease with increasing k, advection overwhelms propagation (so that $c_{22} > c_{11}$) beyond point C in Fig. 1. To make the phase speeds more similar, the CRWs have to phase-lock such that they increase the counter-propagation rate of each other (i.e. they 'help' each other to propagate against the shear). This 'helping' is achieved by making the CRW phase-difference less than $\pi/2$. Oppositely, for $k < 1.88$ the CRWs phase-lock in an increasingly 'hindering' configuration ($\epsilon > \pi/2$).

At a particular wavenumber, phase-locking cannot be maintained in time, unless the CRWs are either π out of phase (marking the long-wave cut-off, point A in Fig. 1) or completely in phase (marking the short-wave cut-off, point D in Fig. 1). For the two-layer Eady model, the linearly amplifying solutions discussed in the previous sections are found at these cut-off wavenumbers.

4.1. Phase-space evolution

All initial-value experiments relevant for system (3) for a fixed set of parameters can be summarized in a phase diagram. The phase space is two-dimensional, since the CRW phase difference ϵ and the CRW amplitude ratio χ are sufficient to describe the evolution unambiguously. The evolution equations for χ and ϵ are, however, non-linear [see also Heifetz et al., (2004a), their eqs 45a and b]:

$$\dot{\chi} = \sigma\left(1 - \chi^2\right)\sin\epsilon\ , \quad \dot{\epsilon} = \mu + \sigma\left(\chi + \chi^{-1}\right)\cos\epsilon. \tag{18}$$

Trajectories for (18) are constructed easily, noting the two time-invariants of the system (Davies and Bishop, 1994):

$$\frac{\mathrm{d}}{\mathrm{d}t}\left(a_1^2 - a_2^2\right) = 0, \quad \frac{\mathrm{d}}{\mathrm{d}t}\left(a_1^2 + a_2^2 + \frac{4\sigma}{\mu}a_1 a_2 \cos\epsilon\right) = 0, \tag{19}$$

where a_i are the real amplitudes of the CRWs (see eq. 2). The line $\chi = 1$ ($a_1 = a_2$) is special. If $\chi = 1$ initially, then $\chi = 1$ at all subsequent times, and only the phase-difference changes in time. Then the evolution is called 'synchronous' (Davies and Bishop, 1994). In the growing regime, this behaviour causes synchronous growth. In the neutral regime, there are periods of synchronous growth (when $0 \le \epsilon \le \pi$) and synchronous decay (when $-\pi \le \epsilon \le 0$), which is clearly remarkable since both underlying NMs have amplitude ratios differing from $\chi = 1$ (see also Fig. 2; a discussion follows in the next section). In Appendix B, analytic expressions are obtained for the synchronous problem in the case of marginal neutrality.

In the subsequent sections, we show the scaled amplitude ratio $\xi \equiv (4/\pi)\arctan(\chi)$ rather than χ. The variable ξ maps $\chi \in [0, \infty]$ to $\xi \in [0, 2]$, while $\xi = 1$ remains equivalent to $\chi = 1$. To better appreciate the continuous transition from one part of the dispersion diagram into another, we will start with short neutral waves and gradually decrease the wavenumber.

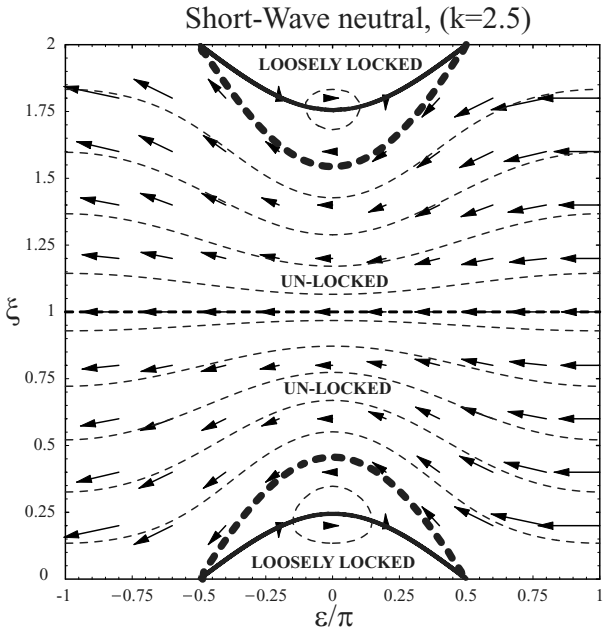

Fig. 2. Phase diagram for short neutral waves. The horizontal axis represents the CRW phase-difference ϵ/π, the vertical axis the scaled CRW amplitude ratio $\xi = (4/\pi)\arctan\chi$. Arrows indicate the flow in the phase diagram, and some trajectories are shown by dashed lines. Dashed thick lines denote limit trajectories. Thick solid lines represent the 'turning points' where $\dot{\epsilon} = 0$.

4.2. Short neutral waves

As indicated by the dispersion diagram (Fig. 1), there are no unstable waves in the short-wave limit. In the phase diagram (Fig. 2), this becomes manifest by the the absence of any attracting fixed points.

Instead, two stable centres (the two neutral NMs) form at the points where the $\dot{\epsilon} = 0$ lines (thick full) meet the $\dot{\xi} = 0$ lines (where $\epsilon = 0$ or $\epsilon = \pm\pi$). As has been discussed in the previous section, the CRWs phase lock in the short neutral NMs in a fully 'helping' configuration with $\epsilon = 0$.

Outside the fixed-points, phase-plane trajectories take the form of either two 'unlocked' or of two 'loosely-locked' CRWs.

In the unlocked regime, the upper CRW propagates eastwards faster than the lower CRW, which is indicated by all arrows pointing toward the left-hand side. The arrows generally are largest near $\epsilon = \pm\pi$, corresponding to situations of maximally hindering configuration. In the loosely-locked regime, the lower and upper CRW maxima are never further apart than $\pm\pi/2$, and they continuously take over and are being taken over by the other CRW. Whether the stable centres (i.e. the NMs) have counter-clockwise or clockwise moving trajectories, depends on whether the amplitude ratio ξ is smaller or greater than 1.

The line $\xi = 1$, associated with the synchronous problem, splits the phase plane into an upper and lower half-plane. This observation holds for both stable and unstable wavenumber regimes. Evolution necessarily takes place in either of the two half-planes and trajectories, therefore, never cross (but may end at) the line $\xi = 1$.

A limit trajectory (shown as the thick dashed line) separates the two trajectory types, somewhat similar to a separatrix. These limit trajectories (thick dashed lines) are special. In these cases, one of the two CRWs will periodically decay to zero amplitude as the CRW relative phase-difference approaches $\epsilon = -\pi/2$ (configuration for optimal instantaneous decay). It then 'reappears', but obviously ϵ has changed to $\pi/2$ (configuration for optimal instantaneous growth) and the cycle is repeated.

4.3. Short marginal waves

When the wavenumber is decreased, more and more trajectories will be of the 'loosely-locked' type. The dashed thick lines of Fig. 2 get closer and closer, implying that the 'un-locked' trajectories become increasingly undulated toward $\xi = 1$ near $\epsilon = 0$. It is as if the appearance of an unstable NM with $\chi = 1$ is somehow being prepared. When the two limit trajectories finally meet at $(\epsilon, \xi) = (0, 1)$, as shown in Fig. 3, the short-wave cut-off is reached.

It does not make sense, any longer, to speak of 'loosely-locked' or 'unlocked' trajectories. We are at the short-wave resonant limit, whose properties were discussed in detail in Section 3. Even though the mNM is neutral, all initial conditions, which are but slightly different in structure from the mNM, eventually end up in $(\epsilon, \xi) = (0, 1)$, which is the mNM. The mNM point

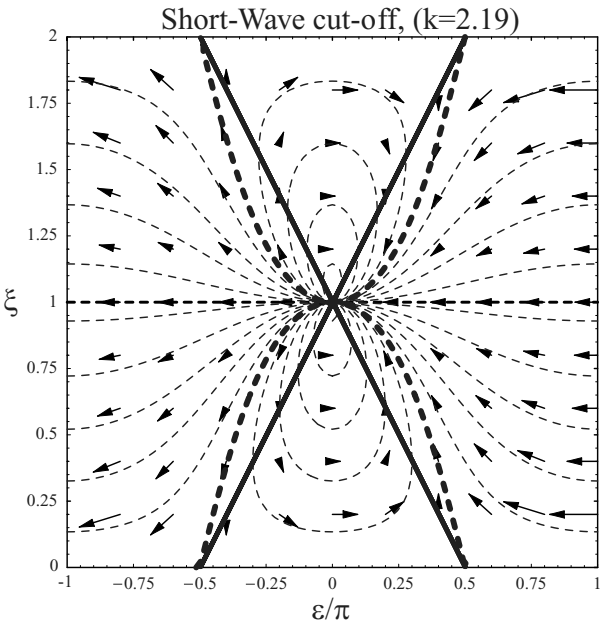

Fig. 3. As in Fig. 2 but for short, but marginally neutral waves. Due to periodicity of ϵ all trajectories eventually end in $(\xi, \epsilon) = (1, 0)$, even though it is a saddle point.

$(\epsilon, \xi) = (0, 1)$ is a saddle point, where non-linearity (in this case the $\sin\epsilon$ term) determines the stability. It is because of the periodic boundary conditions in the zonal direction that all trajectories inevitably end in $(\epsilon, \xi) = (0, 1)$.

4.4. Unstable waves

When the wavenumber is decreased further, the $\dot{\epsilon} = 0$ thick full lines, which formed the X-shaped structure in Fig. 3, separate again, but now in the horizontal. Two unstable fixed points occur, one attracting (the gNM), the other repelling (the dNM). Initially, the fixed points are very close to each other and are found near $(\epsilon, \xi) = (0, 1)$, but they get further apart as the wavenumber is further decreased. This is the classic picture of an exponentially gNM determining the time-asymptotic dynamics.

Rather than showing the phase diagram for the most unstable wave, Fig. 4 displays the phase plane for the resonantly unstable wave for which $c_{11} = c_{22}$ (point C in the dispersion diagram). In this configuration, the $\dot{\epsilon} = 0$ lines have become vertical. Indeed, the gNM is formed by the lower and upper CRW positioned exactly $\pi/2$ out of phase.

4.5. Long marginal and neutral waves

Upon decreasing the wavenumber further, the $\dot{\epsilon} = 0$ lines bend apart further, until they meet again at the long-wave cut-off (point A in the dispersion diagram). Again a saddle point is found (with algebraic linear growth of the mNM) but now at $(\epsilon, \xi) = (\pm\pi, 1)$, see Fig. 5.

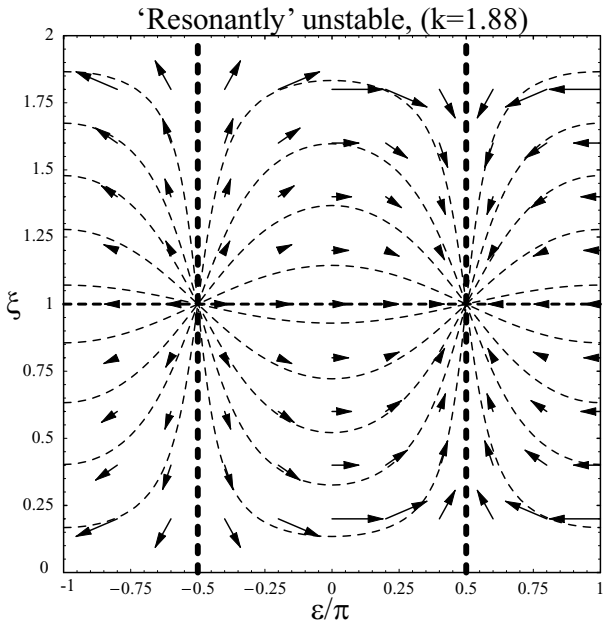

Fig. 4. As in Fig. 2 but for the 'resonantly' unstable waves ($c_{11} = c_{22}$). The $\dot{\epsilon} = 0$ lines coincide with the thick dashed lines and are therefore not shown.

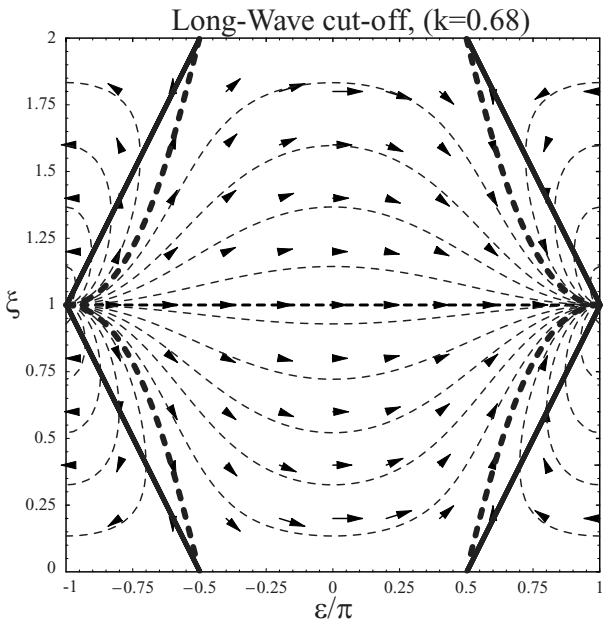

Fig. 5. As in Fig. 2 but for long, marginally neutral waves. Now the saddle point is located at $(\xi, \epsilon) = (1, \pm\pi)$.

Going beyond the long-wave cut-off, results in situations which are qualitatively similar to the short neutral waves, however, the direction of the arrows in Fig. 5 is opposite, because the propagation of the CRWs relative to the shear is too strong to enable phase-locking. Interestingly, this also occurs at the neutral points in the Charney model (Heifetz et al., 2004b). Similar to the short-wave neutral limit discussed in Fig. 2, there are two types of trajectories, loosely-locked and unlocked, depending on the initial CRW amplitude ratio and phase-difference.

5. Concluding remarks

Parallel shear flows have been shown to support linearly amplifying wave disturbances under circumstances where the dispersion diagram predicts marginal neutrality of NMs. CRW theory has been applied to understand the physical mechanisms underlying the development. It was shown that the sustained linear growth occurs through a resonance mechanism in which the mNM that exists in this limit, is being excited by the initial condition. An analysis of the CRW phase space was added to better appreciate how, in the initial-value problem, there is a continuous, rather than sudden transition—as could be concluded from the dispersion diagram—from one dynamic regime (say baroclinic neutrality) in to another (baroclinic instability), as a wave parameter such as wavenumber changes. The results have been illustrated for the two-layer Eady model. The paper is concluded with some further remarks.

One issue relates to the validity of the Figs. 2–5 for different models. It can be said that these diagrams will be qualitatively

similar for all models whose NM dynamics can be described by two interacting CRWs. Of course, the details will vary: the wavenumbers at which the dynamics takes the particular forms shown in Figs. 2–5, will be model-specific, as will be the lengths of the arrows—the speed with which the trajectories are being followed. Also, the phase difference attained by the CRWs in the mNM will be model-specific. The Charney (1947) problem, for example, does not have a short-wave cut-off (Heifetz et al., 2004b). Instead, the growth rate becomes smaller and smaller, because, as $k \to \infty$ also the interaction coefficient $\sigma \to 0$. From (7), it then follows that the CRWs must phase-lock in the $\pi/2$ 'resonantly' unstable configuration. This short-wave limit is, therefore, different from that obtained here for the two-layer Eady model. On the other hand, for decreasing k, the first neutral point in the Charney problem is reached for CRWs in a fully 'hindering' configuration (i.e. $\epsilon = \pi$), similar to the long-wave cut-off in the two-layer Eady model (cf. Fig. 5).

Another remark is that the resonant solutions are only exact (i.e. valid for infinitely long time) in the marginal neutral limit where $\Gamma = 0$ (see eq. 7). On the other hand, Figs. 2–5 show that there is a continuous transition between the different wavenumber regimes from an initial-value viewpoint. Therefore, it can be expected that the mechanism of the resonant-like linear growth is important—albeit not for infinitely long time—also for near-marginal wavenumbers. The time interval in which this resonance interpretation is valid, obviously depends on the structure of the dispersion diagram near the marginal point. A mathematical verification is given in Appendix C.

As an example of a situation in which the resonance interpretation does make sense, even though it is not valid exactly, Fig. 6 shows a time integration of the CRW equations of the two-layer Eady model, for a wavenumber that is somewhat smaller than the long-wave cut-off. Starting with the CRWs in phase (thereby maximally 'helping' each others propagation against the shear), it is shown that very quickly the disturbance resembles the (linearly amplifying) mNM ($\xi \sim 1, \epsilon \sim \pi$) and remains so for a surprisingly long time, before eventual decay sets in (this happens when the phase-difference becomes greater than π).

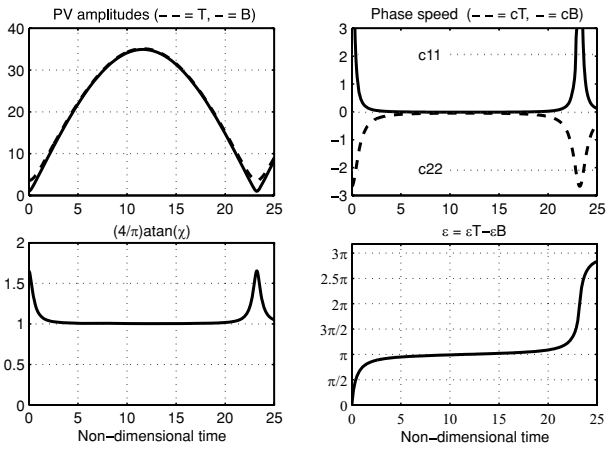

Fig. 6. Initial-value experiment ($q(z_1) = 1, q(z_2) = 4$) for $k = 0.5$, which is smaller than the long-wave cut-off (see Fig. 1). Note that for this wavenumber $c_{11} > c_{22}$.

The previous example emphasizes the importance of linear growth mechanisms for short-term baroclinic development. In this light, it is worth mentioning that there are other ways to get sustained growth through a similar resonance phenomenon. Linear growth for instance also occurs in the Eady problem, if one adds an interior PV anomaly of the form $q = Q\delta(z - h)$ at one of the steering levels of the neutral NMs. At that height, the PV anomaly is able to co-propagate with the neutral NM and simultaneously excite it (Chang, 1992; Dirren and Davies, 2004; De Vries and Opsteegh, 2005; Jenkner and Ehrendorfer, 2006). If the interior PV anomaly is positioned at the steering level of the mNM, a 'double' resonance occurs with associated quadratic growth of the streamfunction. The quadratic growth occurs because the interior PV anomaly linearly excites two boundary CRWs, which in turn excite the underlying mNM (see also Appendix A).

To conclude, the present paper has shown that, even though the NMs change in a fundamental way as wave parameters are varied (such that bifurcations occur), initial-value experiments can be understood remarkably well. This understanding was achieved essentially because the CRW phase space transits smoothly from one regime to another, with the resonant-like growth forming a bridge (not a singular point) between exponential instability and baroclinic neutrality. On the basis of this understanding of the present prototypical situation, our understanding of the variability and development of real baroclinic weather systems in the atmosphere is also improved.

Acknowledgments

Two anonymous reviewers are thanked for their careful reading of the manuscript. The authors have appreciated discussions with John Methven, Tom Frame and Brian Hoskins. This work was supported by the National Environmental Research Council (NERC, grant NE/D011507/1), the Netherlands Organisation for Scientific Research (NWO, Rubicon grant) and the NERC Data Assimilation Research Centre (DARC). The idea for the paper originated when HdV was visiting University of Innsbruck in 2007.

Appendix A: The Jordan form

A.1. Multiplicity two eigenvalues: linear growth

When $\Gamma = 0$, the matrix $\mathbf{A}$ in (3) is similar to the Jordan matrix $\mathbf{J}$ in (11) through the transformation:

$$\mathbf{A} = \mathbf{T}\mathbf{J}\mathbf{T}^{-1}, \quad \mathbf{T} = \begin{pmatrix} -\rho_c & -k/\sigma \\ 1 & 0 \end{pmatrix}, \tag{A1}$$

where ρ_c was defined in (8). The first column of matrix $\mathbf{T}$ represents the single eigenvector of matrix $\mathbf{A}$ corresponding to the single eigenvalue $\bar{c}$ of multiplicity 2.

A.2. Multiplicity three eigenvalues: quadratic growth

Assume we locate an interior PV delta function at the steering level of the mNM in the Eady problem. In that case, the resulting 3×3 eigenvalue problem has one eigenvalue of multiplicity 3. The Jordan matrix and the transformation matrix are then given by

$$\mathbf{J}_3 = \begin{pmatrix} \bar{c} & 1 & 0 \\ 0 & \bar{c} & 1 \\ 0 & 0 & \bar{c} \end{pmatrix}, \mathbf{T}_3 = \begin{pmatrix} -\rho_c & -k/\sigma & -ak^2/\sigma^2 \\ 1 & 0 & 0 \\ 0 & 0 & -bk/\sigma \end{pmatrix}, \quad \text{(A2)}$$

where $a = c_{23}/(c_{13} + \rho_c c_{23})$ and $b = 1/(c_{13} + \rho_c c_{23})$. The factors c_{13} and c_{23} are defined in the same way as the c_{ij} for $(i, j) \in (1, 2)$ and the subscript 3 refers to the position and structure of the PV delta-function. As expected, $\mathbf{J}_3$ and $\mathbf{T}_3$ contain $\mathbf{J}$ and $\mathbf{T}$, respectively, as submatrices. The solution in Jordan space becomes (cf. eq. 11):

$$\boldsymbol{\beta}(t) = \mathrm{e}^{-\mathrm{i}k\bar{c}t} \begin{pmatrix} 1 & -\mathrm{i}kt & -\frac{1}{2}k^2t^2 \\ 0 & 1 & -\mathrm{i}kt \\ 0 & 0 & 1 \end{pmatrix} \boldsymbol{\beta}(0). \quad \text{(A3)}$$

The quadratic growth vanishes only if $\beta_3(0) = 0$. The linear growth vanishes also if additionally $\beta_2(0) = 0$, as discussed in Section 3.3.

Note that if $\rho_c = 1$, the special case $c_{13} = -c_{23}$ is not correctly described by (A2). This was expected, since in that case the interior PV anomaly excites precisely the mNM. Therefore, J_3 and T_3 take a different form (not shown) and the quadratic growth is replaced by a linear growth. In other words, a quadratic growth only results if the interior PV anomaly creates boundary CRW anomalies that are not equal to the mNM.

Appendix B: Synchronous initial-value problem

If the initial CRW amplitudes are equal, system (3) simplifies to (Davies and Bishop, 1994; Heifetz et al., 2004a)

$$\dot{a} = \sigma a \sin\epsilon, \qquad \dot{\epsilon} = \mu + 2\sigma\cos\epsilon, \quad \text{(B1)}$$

where $a_1 = a_2 \equiv a$. At the point of marginal stability (cf. eq. 8), (B1) is solved as

$$a(t) = a_0 \left[\frac{1 + (c_0^{\pm} + 2\sigma t)^2}{1 + (c_0^{\pm})^2}\right]^{1/2}, \quad (\rho_c = \pm 1) \quad \text{(B2)}$$

$$\epsilon(t) = 2\mathrm{arctan}(c_0^{+} + 2\sigma t), \quad (\rho_c = +1) \quad \text{(B3)}$$

$$\epsilon(t) = 2\mathrm{arccot}(c_0^{-} + 2\sigma t) \quad (\rho_c = -1), \quad \text{(B4)}$$

where $c_0^{\pm} = [\tan(\epsilon_0/2)]^{\pm 1}$ (for $\rho_c = \pm 1$) is determined by the initial CRW-phase difference ϵ_0. As the perturbation gets large amplitude, the phase-difference asymptotes to either $\epsilon = 0$ (if $\mu = -2\sigma \le 0$) or $\epsilon = \pi$ (if $\mu = 2\sigma \ge 0$) of the underlying mNM. Moreover, note that $a(t)$ increases more rapidly (due to the resonance) if the initial amplitude a_0 is large.

Appendix C: Evolution near the marginal point

Here we show that there is a continuous transition to the linear growth limit, implying that the linear growth regime remains valid at least qualitatively (and for finite time) outside the marginal point. We take a pure CRW-2 initial perturbation described by

$$\boldsymbol{\alpha}(t_0)\sin(kx) = (0, T_0)^{\mathrm{T}} \sin(kx), \quad \text{(C1)}$$

where the T denotes transposition. In the following, we assume that the mNM is described by $(\alpha_1, \alpha_2) = (1, 1)$ (corresponding to the case $\rho_c = -1$ in the main text).

C.1. Limit of two unstable waves

Consider the limit of vanishingly small (but non-zero) gNM growth rate $\hat{\sigma} = \sigma \sin\epsilon_+$ and assume that $\epsilon_+ \sim 0$. Without loss of generality, the gNM and dNM structures can be written as

$$\mathbf{x_1} = \mathrm{e}^{\hat{\sigma}t}\,(1, \mathrm{e}^{\mathrm{i}\epsilon_+})^{\mathrm{T}}\,\mathrm{e}^{\mathrm{i}k(x-\bar{c}t)}, \quad \text{(C2)}$$

$$\mathbf{x_2} = \mathrm{e}^{-\hat{\sigma}t}\left(1, \mathrm{e}^{-i\epsilon_+}\right)^{\mathrm{T}}\mathrm{e}^{\mathrm{i}k(x-\bar{c}t)}. \quad \text{(C3)}$$

It follows that the evolution of the initial disturbance $\boldsymbol{\alpha}$ in (C1) is given by

$$\boldsymbol{\alpha}(t) = T_0 \frac{\mathrm{Re}[\mathbf{x}_2 - \mathbf{x}_1]}{2\sin(\epsilon_+)}. \quad \text{(C4)}$$

A key observation to make is that as the NMs have increasingly more similar structure, the amplitude that both NMs need to have to create a finite amplitude initial disturbance increases $\sim 1/\sin\epsilon_+$. This is similar to the singular behaviour of the continuum modes near the steering level of the surface edge wave in the semi-infinite Eady problem (De Vries and Opsteegh, 2005).

Taking the limits $\epsilon_+ \to 0$ and $\hat{\sigma} \to 0$, while assuming that $\hat{\sigma}/\epsilon_+$ remains finite, gives

$$\alpha_1 = -T_0\left(\frac{\hat{\sigma}t}{\epsilon_+}\right)\left\{\cos[k(x-\bar{c}t)] + O[(\sigma t)^2]\right\}, \quad \text{(C5)}$$

$$\alpha_2 = -T_0\left(\frac{\hat{\sigma}t}{\epsilon_+}\right)\cos[k(x-\bar{c}t)] + T_0\sin[k(x-\bar{c}t)]. \quad \text{(C6)}$$

The above derivation shows how the resonance naturally appears from a consideration of two unstable normal modes in the limit of zero growth rate.

C.2. Limit of two neutral modes

Assume now that we are on the neutral side of the dispersion curve and approach the marginal point. Without loss of generality, we write these two NMs as

$$\mathbf{x}_1 = \mathrm{e}^{\mathrm{i}\omega t}(1, 1-\delta)^{\mathrm{T}}\mathrm{e}^{\mathrm{i}k(x-\bar{c}t)}, \tag{C7}$$

$$\mathbf{x}_2 = \mathrm{e}^{-\mathrm{i}\omega t}(1, 1+\delta)^{\mathrm{T}}\mathrm{e}^{\mathrm{i}k(x-\bar{c}t)}, \tag{C8}$$

where ω/k is the slight change in phase-speed between the neutral NMs and δ accounts for their slightly different vertical structure. The evolution of the initial disturbance (C1) in this case is described by

$$\boldsymbol{\alpha}(t) = T_0 \frac{\mathrm{Re}[-\mathrm{i}(\mathbf{x}_2 - \mathbf{x}_1)]}{2\delta}, \tag{C9}$$

Again, the NM projection coefficients increase (indefinitely) to correctly represent the initial disturbance.

Upon taking the limits $\delta \to 0$ and $\omega \to 0$ (now keeping ω/δ finite) we finally get

$$\alpha_1 = -T_0 \left(\frac{\omega t}{\delta}\right) \left\{\cos[k(x-\bar{c}t)] + O[(\omega t)^2]\right\}, \tag{C10}$$

$$\alpha_2 = -T_0 \left(\frac{\omega t}{\delta}\right) \cos[k(x-\bar{c}t)] + T_0 \sin[k(x-\bar{c}t)]. \tag{C11}$$

Therefore, also the limit of two neutral normal modes reproduces the resonance.

A similar derivation can be performed for any initial condition. It will then follow that unless the initial disturbance is already equal to the mNM, a linear growth will occur. From the 'neutral' point of view, the resonance is interpreted as the infinitely slow unshielding of two infinitely large neutral NMs. From the 'unstable' point of view, the resonance is understood as the infinitely slowly taking over of the gNM in the presence of an equally large, infinitely slowly decaying NM.

C.3. General solution of the initial-value problem

The results of the previous section are confirmed by looking at the general solution of the 2×2 complex system (3):

$$\begin{aligned}
\alpha_1(t)\mathrm{e}^{\mathrm{i}k\bar{c}t} &= B_0 \cosh(\mathrm{d}t/2) - \mathrm{i}(\mu B_0 + 2\sigma T_0)\frac{\sinh(\mathrm{d}t/2)}{\mathrm{d}}, \\
\alpha_2(t)\mathrm{e}^{\mathrm{i}k\bar{c}t} &= T_0 \cosh(\mathrm{d}t/2) + \mathrm{i}(\mu T_0 + 2\sigma B_0)\frac{\sinh(\mathrm{d}t/2)}{\mathrm{d}},
\end{aligned} \tag{C12}$$

where $d^2 \equiv (4\sigma^2 - \mu^2)$ and $\alpha_1(0) = B_0$ and $\alpha_2(0) = T_0$ represents the initial condition. It is easily verified that the resonant solutions (13) and (14) are obtained in the limit $d \to 0$. For $d^2 < 0$ the solutions will be oscillatory, whereas for $d^2 > 0$ they will be growing or decaying. Since the limit $d \to 0$ is well defined and equal from both $d < 0$ and $d > 0$, the transition is said to be smooth.

References

Boyce, W. and DiPrima, R. 2003. *Elementary Differential Equations and Boundary Value Problems* 7th Edition. John Wiley and Sons, Inc. USA.

Bretherton, F. P. 1966. Critical layer instability in baroclinic flows. *Quart. J. Roy. Meteor. Soc.* **92**, 325–334.

Chang, E. K. M. 1992. Resonating neutral modes of the Eady model. *J. Atmos. Sci.* **49**, 2452–2463. Baroclinic instability, Cyclogenesis, Neutral.

Charney, J. G. 1947. The dynamics of long waves in a baroclinic westerly current. *J. Atmos. Sci.* **4**, 135–162.

Charney, J. G. and Stern, M. E. 1962. On the stability of internal baroclinic jets in a rotating atmosphere. *J. Atmos. Sci.* **19**, 159–172.

Davies, H. C. and Bishop, C. H. 1994. Eady edge waves and rapid development. *J. Atmos. Sci.* **51**, 1930–1946.

De Vries, H. and Opsteegh, J. D. 2005. Optimal perturbations in the Eady model: resonance versus PV unshielding. *J. Atmos. Sci.* **62**(2), 492–505.

De Vries, H. and Opsteegh, J. D. 2007. Interpretation of discrete and continuum modes in a two-layer Eady model. *Tellus* **59A**, 182–197.

Dirren, S. and Davies, H. C. 2004. Combined dynamics of boundary and interior perturbations in the Eady setting. *J. Atmos. Sci.* **61**, 1549–1565.

Eady, E. T. 1949. Long waves and cyclone waves. *Tellus* **1**, 33–52.

Fjørtoft, R. 1951. Stability properties of large-scale atmospheric disturbances. In: *Compendium of Meteorology*. American Meteorological Society, Boston, USA.

Green, J. S. A. 1960. A problem in baroclinic stability. *Quart. J. Roy. Meteor. Soc.* **86**, 237–251.

Heifetz, E. and Methven, J. 2005. Relating optimal growth to counterpropagating Rossby waves in shear instability. *Physics of Fluids* **17**(1), 1–14.

Heifetz, E., Bishop, C. H., Hoskins, B. J. and Methven, J. 2004a. The counter-propagating Rossby-wave perspective on baroclinic instability, I: mathematical basis. *Quart. J. Roy. Meteor. Soc.* **130**, 211–231.

Heifetz, E., Methven, J., Hoskins, B. J. and Bishop, C. H. 2004b. The counter-propagating Rossby-wave perspective on baroclinic instability, II: application to the Charney model. *Quart. J. Roy. Meteor. Soc.* **130**, 233–258.

Hoskins, B. J., McIntyre, M. E. and Robertson, A. W. 1985. On the use and significance of isentropic potential vorticity maps. *Quart. J. Roy. Meteor. Soc.* **111**, 877–946.

Jenkner, J. and Ehrendorfer, M. 2006. Resonant continuum modes in the Eady model with rigid lid. *J. Atmos. Sci.* **63**(2), 765–773.

Methven, J., Heifetz, E., Hoskins, B. J. and Bishop, C. H. 2005. The counter-propagating Rossby-wave perspective on baroclinic instability, III: primitive-equation disturbances on the sphere. *Quart. J. Roy. Meteor. Soc.* **131**, 1393–1424.

Müller, J. C. 1991. Baroclinic instability in a two-layer, vertically semi-infinite domain. *Tellus* **43A**, 275–284.

Pedlosky, J. 1987. *Geophysical Fluid Dynamics* 2nd Edition. Prentice Hall, NJ.